Writing: Style, Visualization & Pitfalls

University of Arizona
UBRP Summer 2008

Christopher Bergevin

Department of Mathematics

Overview

1. Finding one’s own ‘*style*’

2. Good (and bad) graphical practice

3. Common pitfalls to avoid

What is style?

Style *vs* Substance

Examples:

	Style	Substance
Speech:	accent, slang	topic, language
Printed Text:	typeface, words	content, ideas
This Presentation:	slides, my voice	message

"Nothing we do can be done 'simply' and in no style, because style is something inherent in action, not something added to it."

- Thomas and Turner

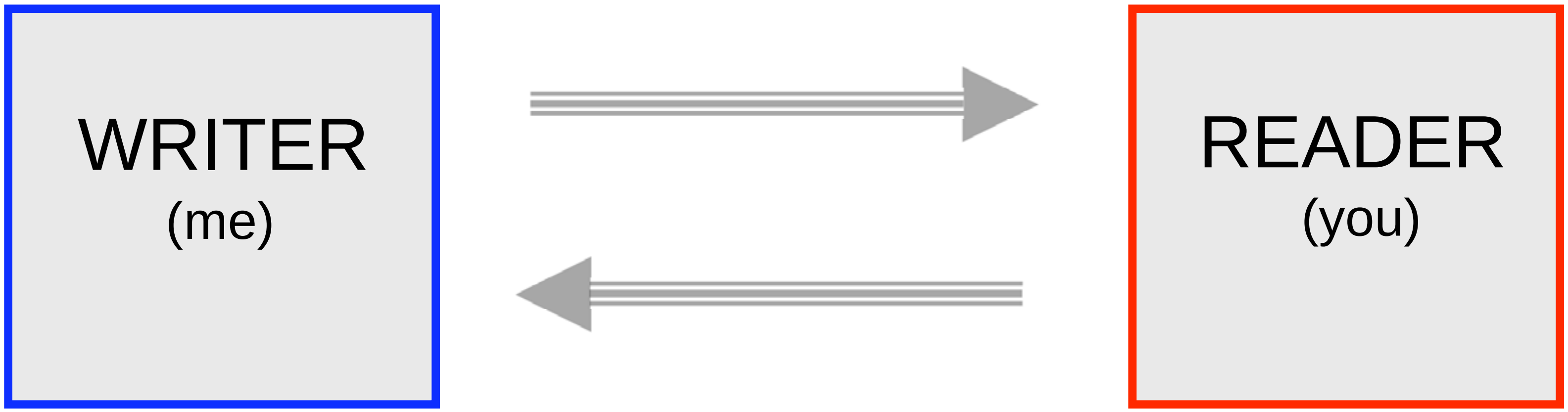

Cast a role both for yourself and the reader

Classic style

‘Mon style ne sera point fleuri, mes expressions seront simples comme la vérité.’

- Jean-Baptiste Le Brun (1700’s)

‘My style will not be at all florid, my expression will be as simple as the truth.’

‘as simple as the truth’

Classic style

Northern Shrike (*Lanius excubitor*)

"Unusual among songbirds, shrikes prey on small birds and rodents, catching them with the bill and sometimes impaling them on thorns or barbed wire for storage. Like other northern birds that depend upon rodent populations, the Northern Shrike movements are cyclical, becoming more abundant in the South when northern rodent populations are low. At times they hunt from an open perch, where they sit motionless until prey appears; at other times they hover in the air ready to pounce on anything that moves."

- Audobon Society Field Guide

Classic style

"Physics has a history of synthesizing many phenomena into a few theories."

- Richard Feynman

Non-Classic style

Fact: Science is full of blood, sweat, tears, details & dead-ends

Ask yourself: Do we do a reader/student a disservice by obscuring that?

⇒ Think about how you want to convey information
i.e. find your own style/voice

Case Study

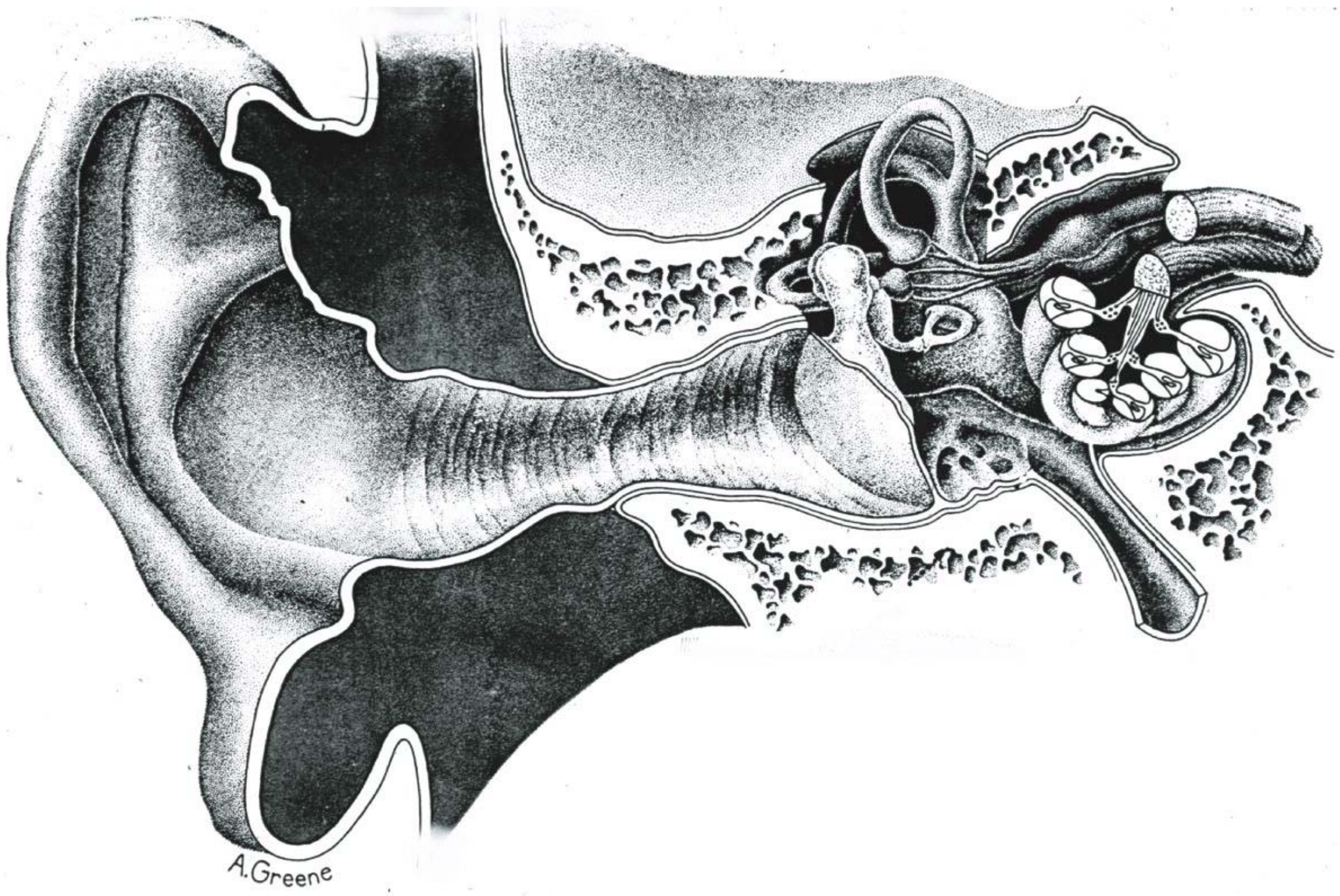

Case Study

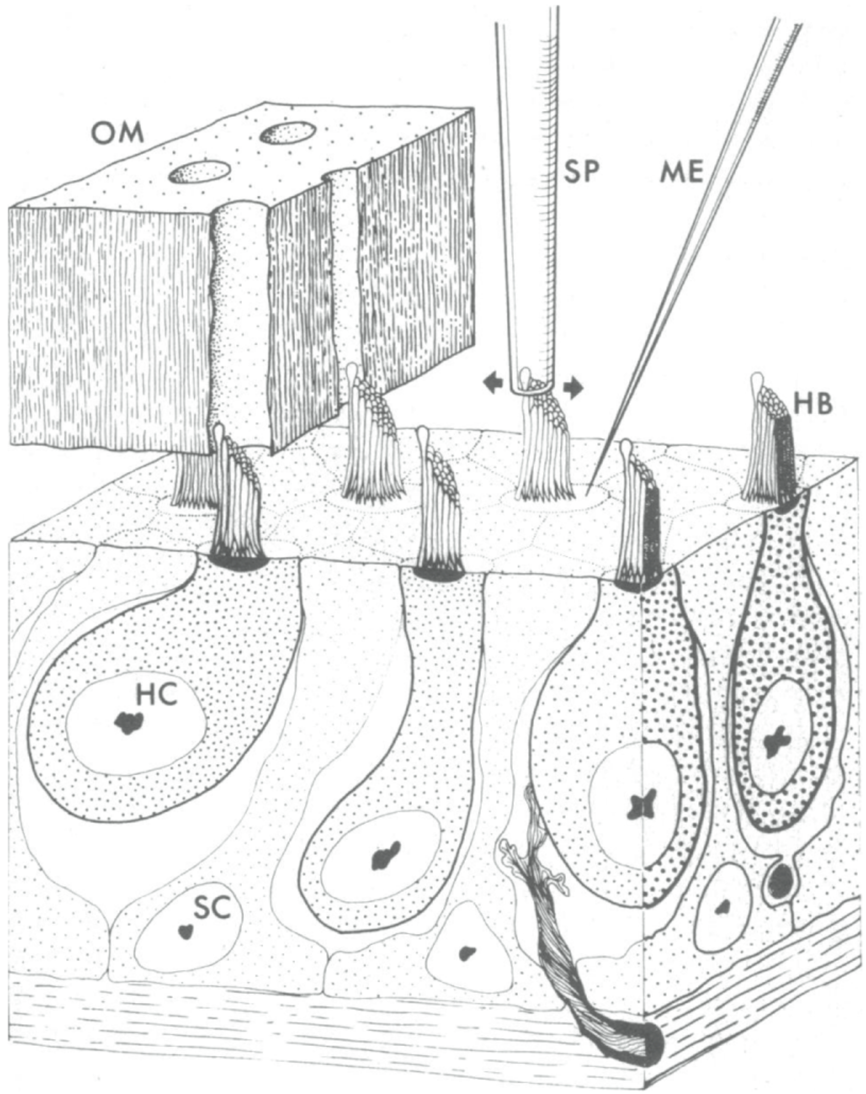

Corey and Hudspeth (1977)

Case Study

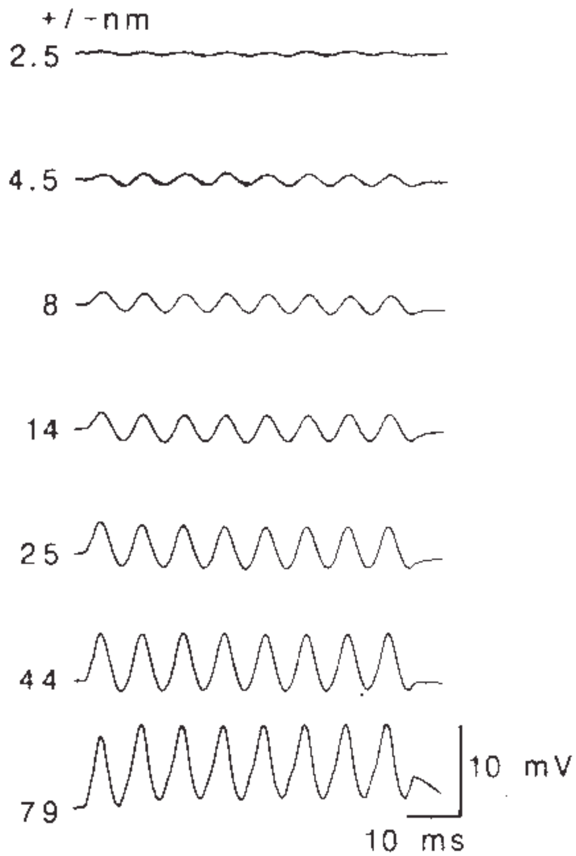

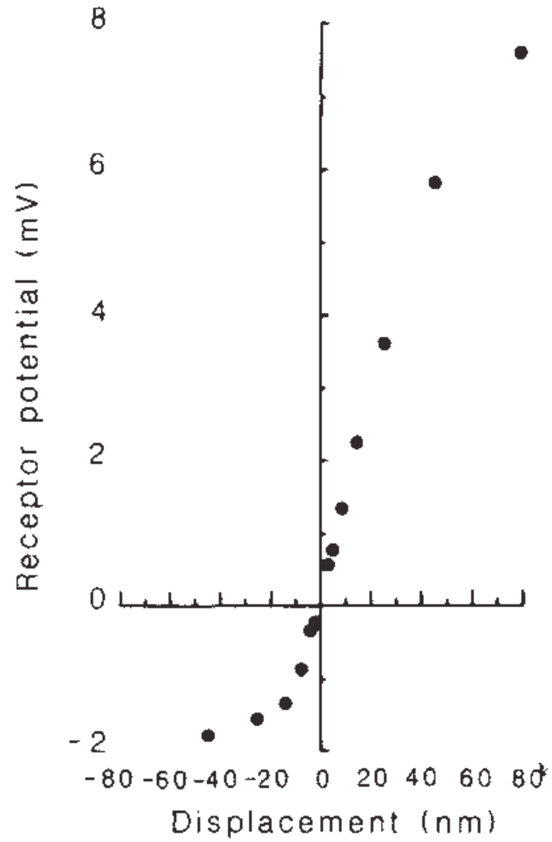

Russell, Richardson and Cody (1986)

Case Study

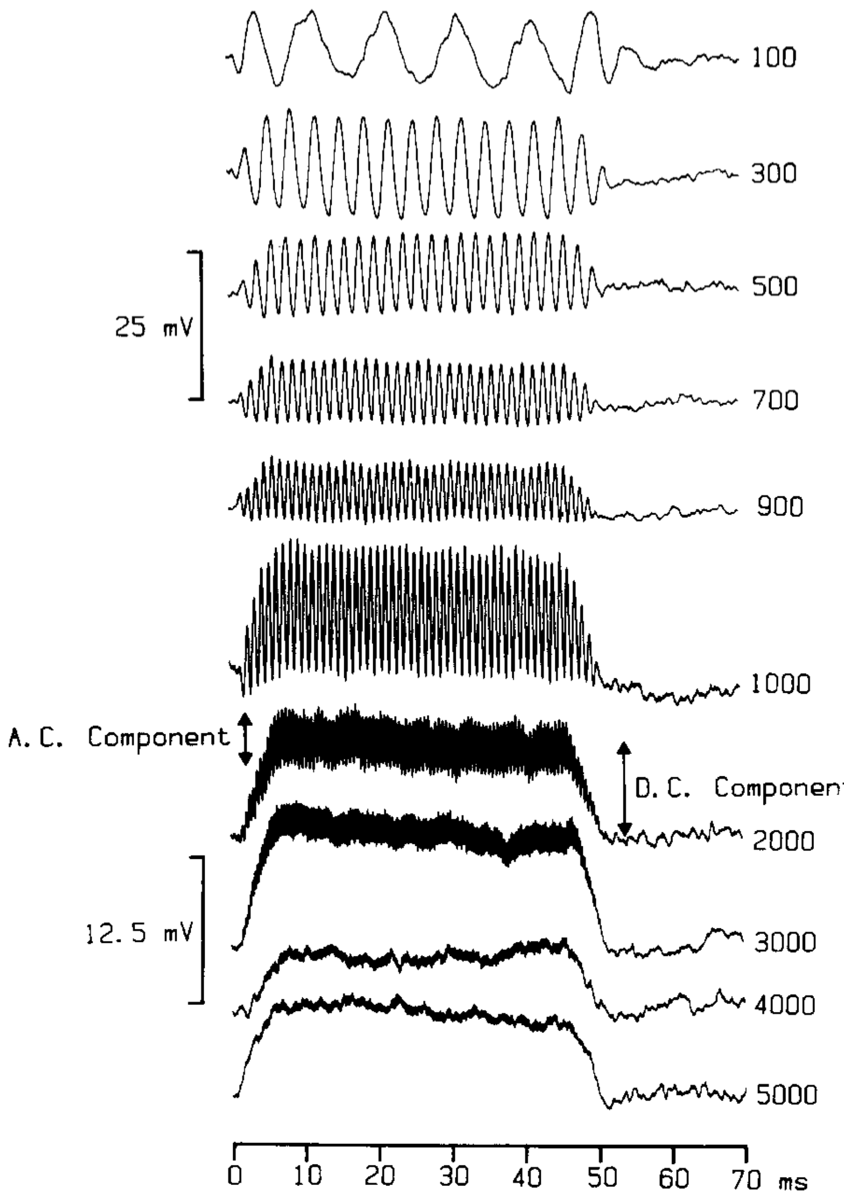

Palmer and Russell (1986)

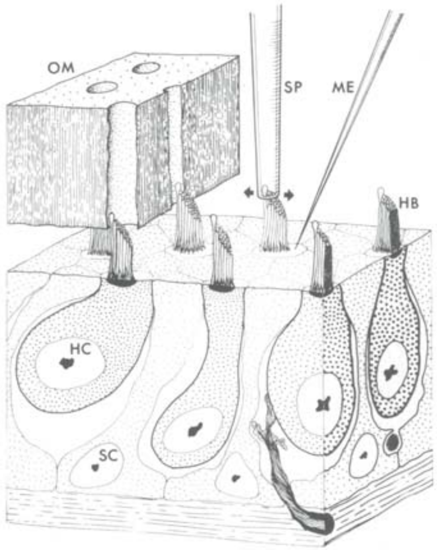

Corey and Hudspeth (1977)

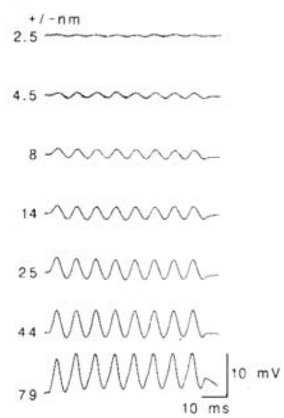

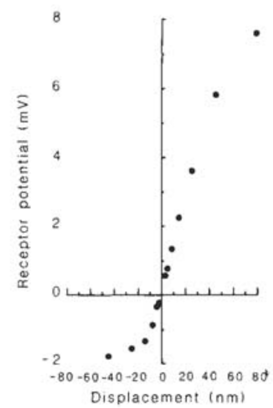

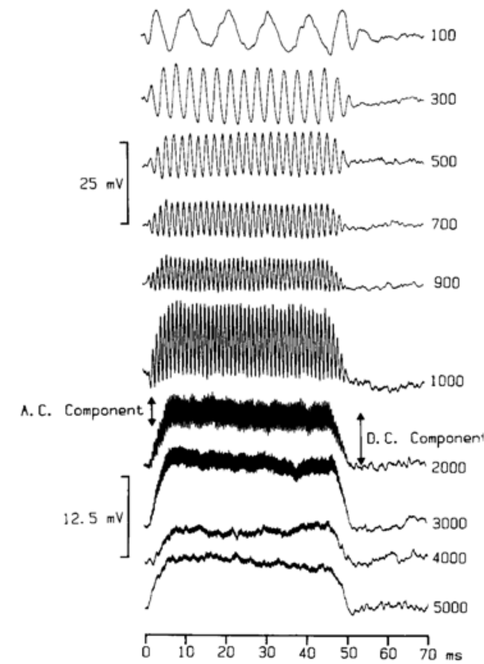

Russell, Richardson and Cody (1986)

<u>Task:</u> come up (with the person next to you) with a title to a report describing your results

Data Visualization

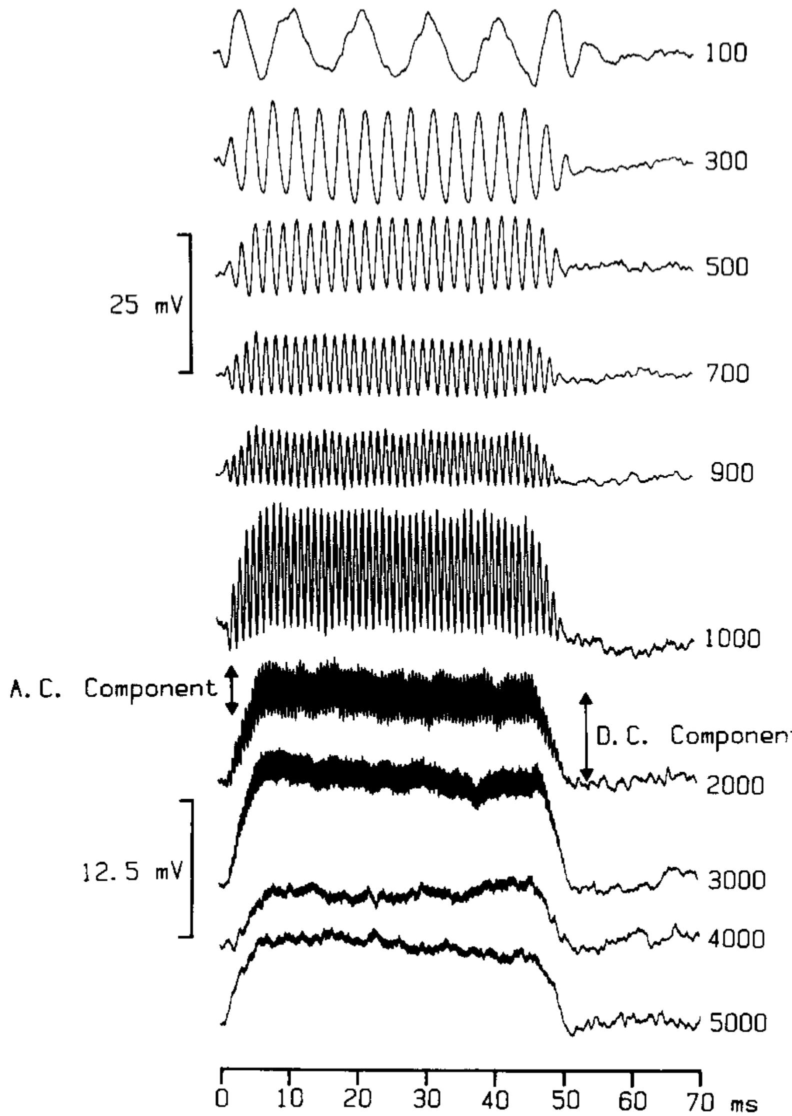

Palmer and Russell (1986)

Principles of '*Graphical Excellence*'

- show the data

- avoid distorting what the data have to say

- make large data sets coherent; present many #s in a small space

- serve a reasonably clear purpose

- reveal the data at several levels of detail

- tell the truth about the data

Principles of *Graphical Excellence*

GOAL: Give the viewer the greatest number of ideas in the shortest amount of time with the least ink in the smallest space

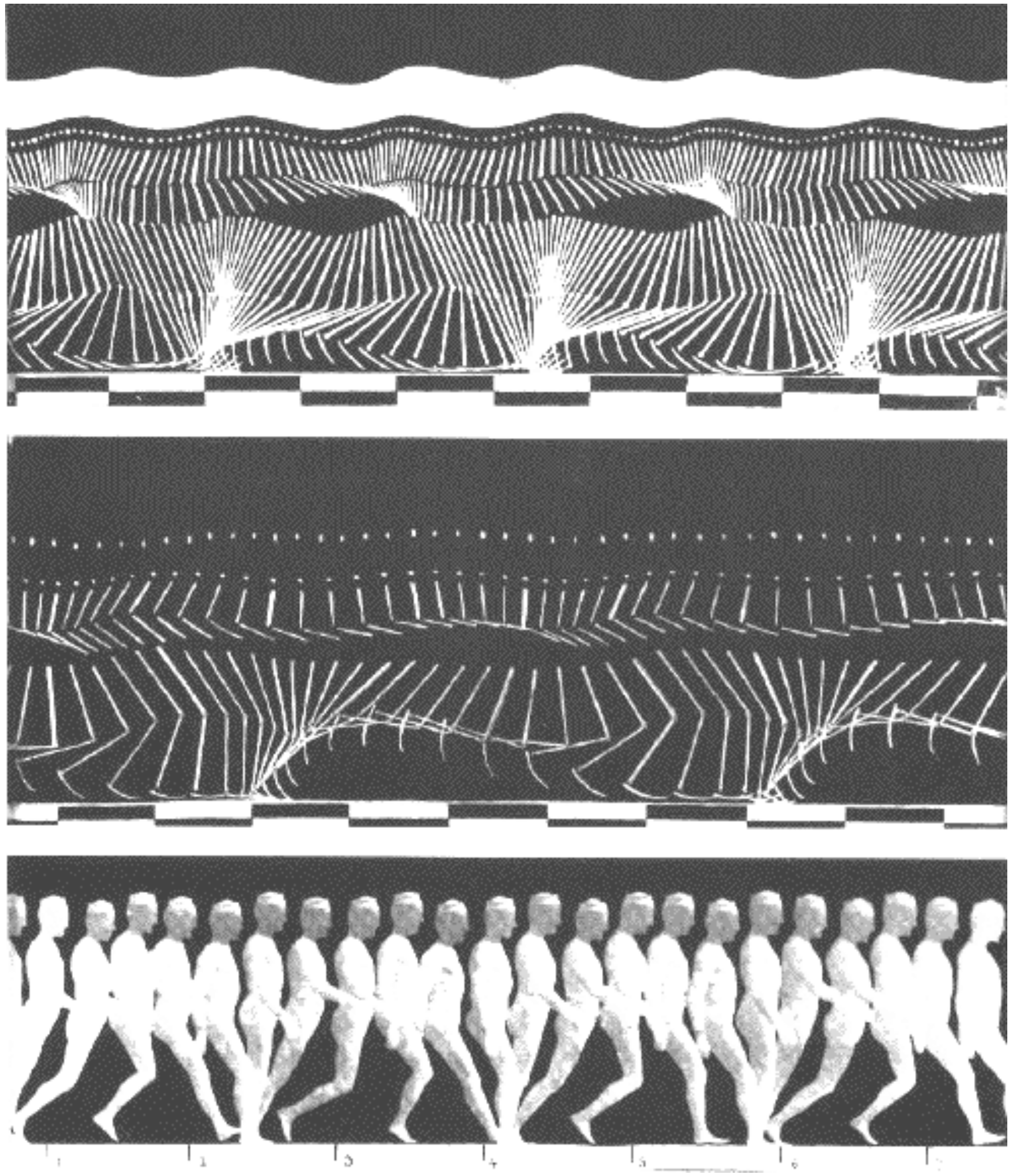

Marey (~1885)

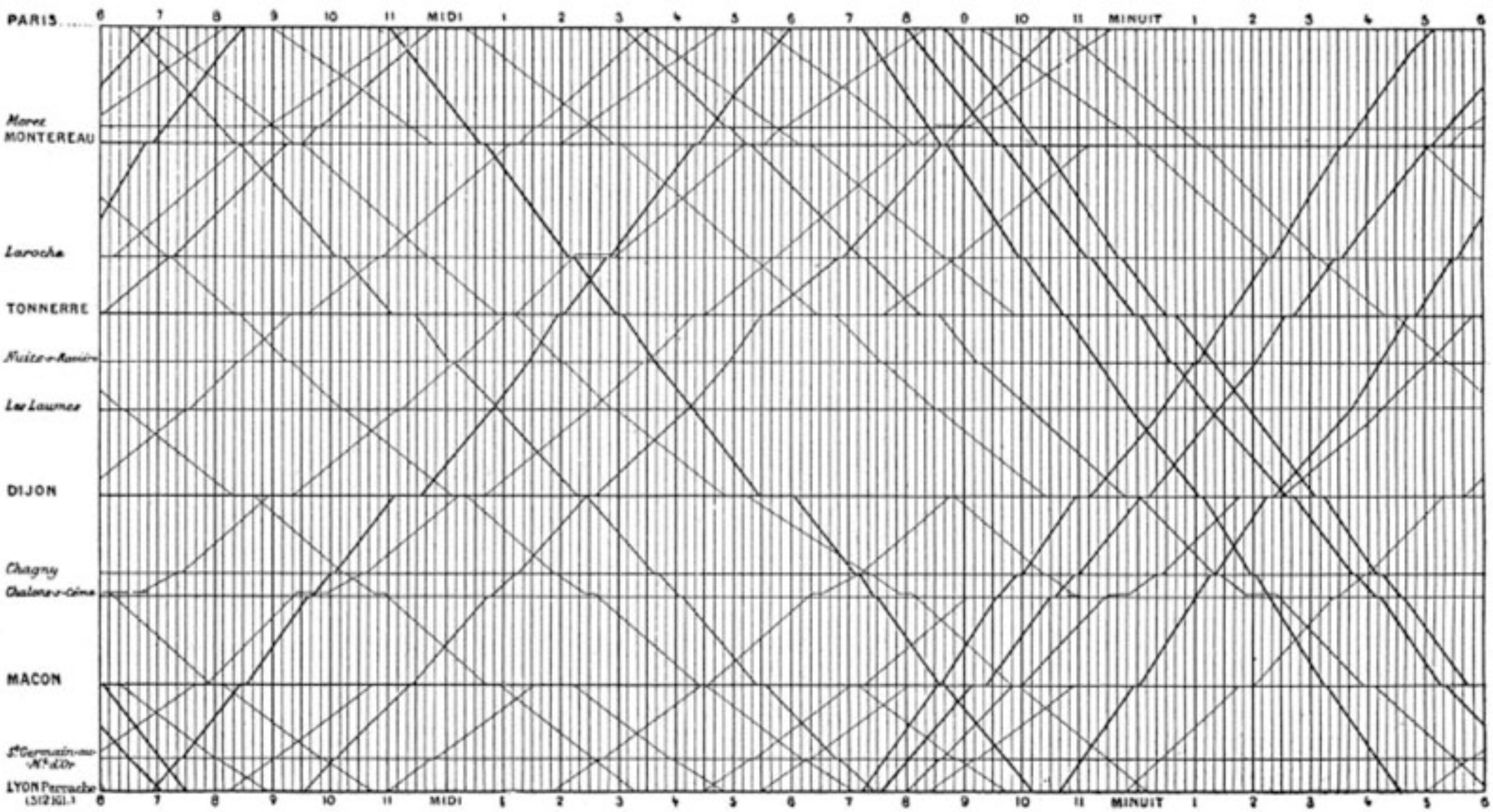
PARIS
MONTEREAU
Laroche
TONNERRE
Les Laumes
DIJON
Chagny
MACON
LYON Perrache
6 7 8 9 10 11 MIDI 1 2 3 4 5 6 7 8 9 10 11 MINUIT 1 2 3 4 5 6

Marey (1880)

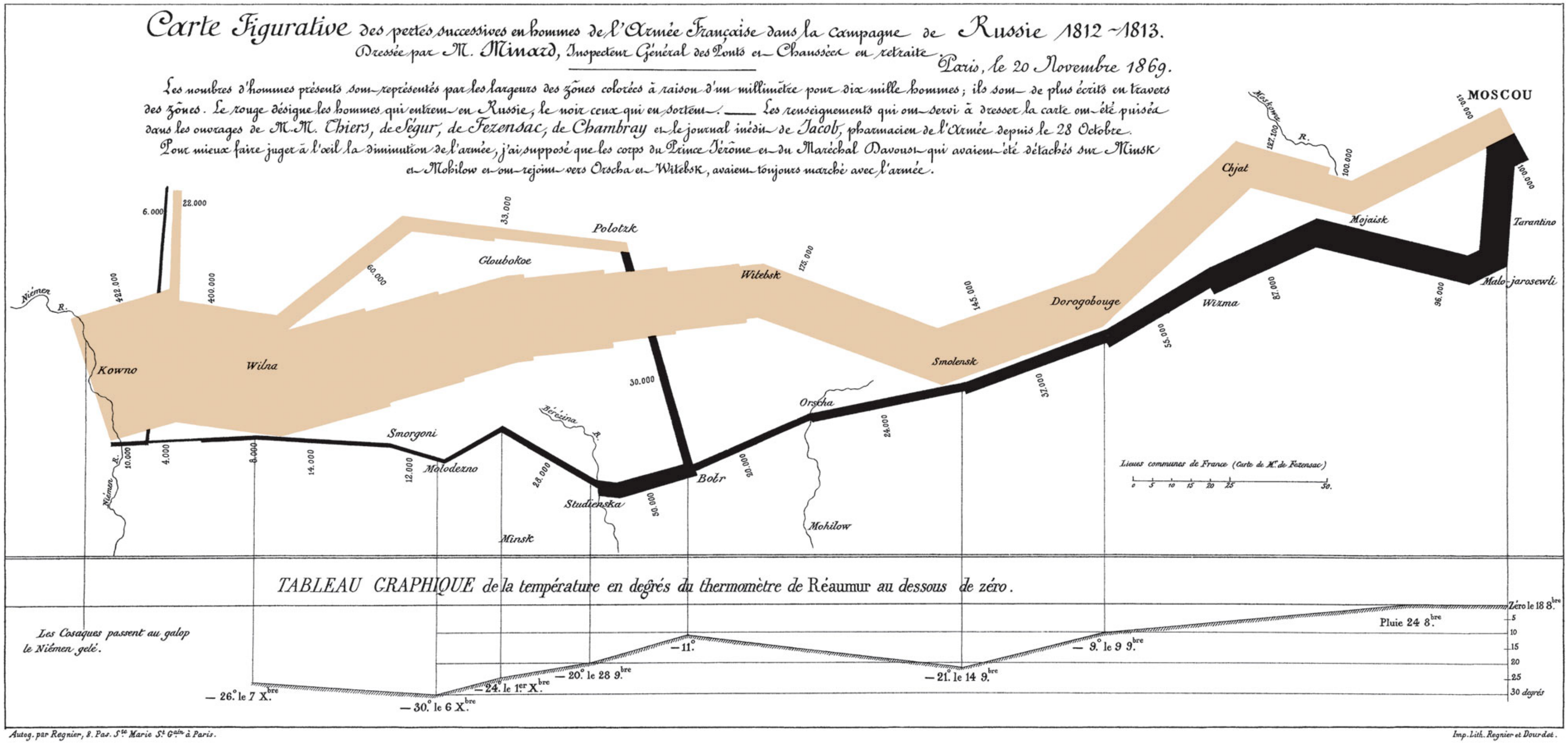
Carte Figurative des pertes successives en hommes de l'Armée Française dans la campagne de Russie 1812–1813.
Dressée par M. Minard, Inspecteur Général des Ponts et Chaussées en retraite.
Paris, le 20 Novembre 1869.
Les nombres d'hommes présents sont représentés par les largeurs des zones colorées à raison d'un millimètre pour dix mille hommes; ils sont de plus écrits en travers des zones. Le rouge désigne les hommes qui entrent en Russie, le noir ceux qui en sortent. —— Les renseignements qui ont servi à dresser la carte ont été puisés dans les ouvrages de M.M. Thiers, de Ségur, de Fezensac, de Chambray et le journal inédit de Jacob, pharmacien de l'Armée depuis le 28 Octobre.
Pour mieux faire juger à l'œil la diminution de l'armée, j'ai supposé que les corps du Prince Jérôme et du Maréchal Davoust qui avaient été détachés sur Minsk et Mohilow et ont rejoint vers Orscha et Witebsk, avaient toujours marché avec l'armée.
MOSCOU
Moskowa R.
Chjat
Mojaisk
Tarantino
Malo-jarosewli
Wizma
Dorogobouge
Smolensk
Orscha
Witebsk
Polotzk
Gloubokoe
Wilna
Kowno
Niémen R.
Smorgoni
Molodezno
Bérézina R.
Studienska
Minsk
Bobr
Mohilow
422.000
400.000
22.000
6.000
60.000
33.000
175.000
145.000
127.100
100.000
100.000
100.000
96.000
87.000
55.000
37.000
24.000
30.000
20.000
50.000
28.000
12.000
14.000
8.000
4.000
10.000
Lieues communes de France (Carte de M. de Fezensac)
0 5 10 15 20 25 50.
TABLEAU GRAPHIQUE de la température en degrés du thermomètre de Réaumur au dessous de zéro.
Les Cosaques passent au galop le Niémen gelé.
Zéro le 18 8.bre
Pluie 24 8.bre
— 9° le 9 9.bre
— 21° le 14 9.bre
— 11°
— 20° le 28 9.bre
— 24° le 1er X.bre
— 30° le 6 X.bre
— 26° le 7 X.bre
5
10
15
20
25
30 degrés
Autog. par Regnier, 8. Pas. Ste Marie St Gain à Paris.
Imp. Lith. Regnier et Dourdet.

Minard (1880)

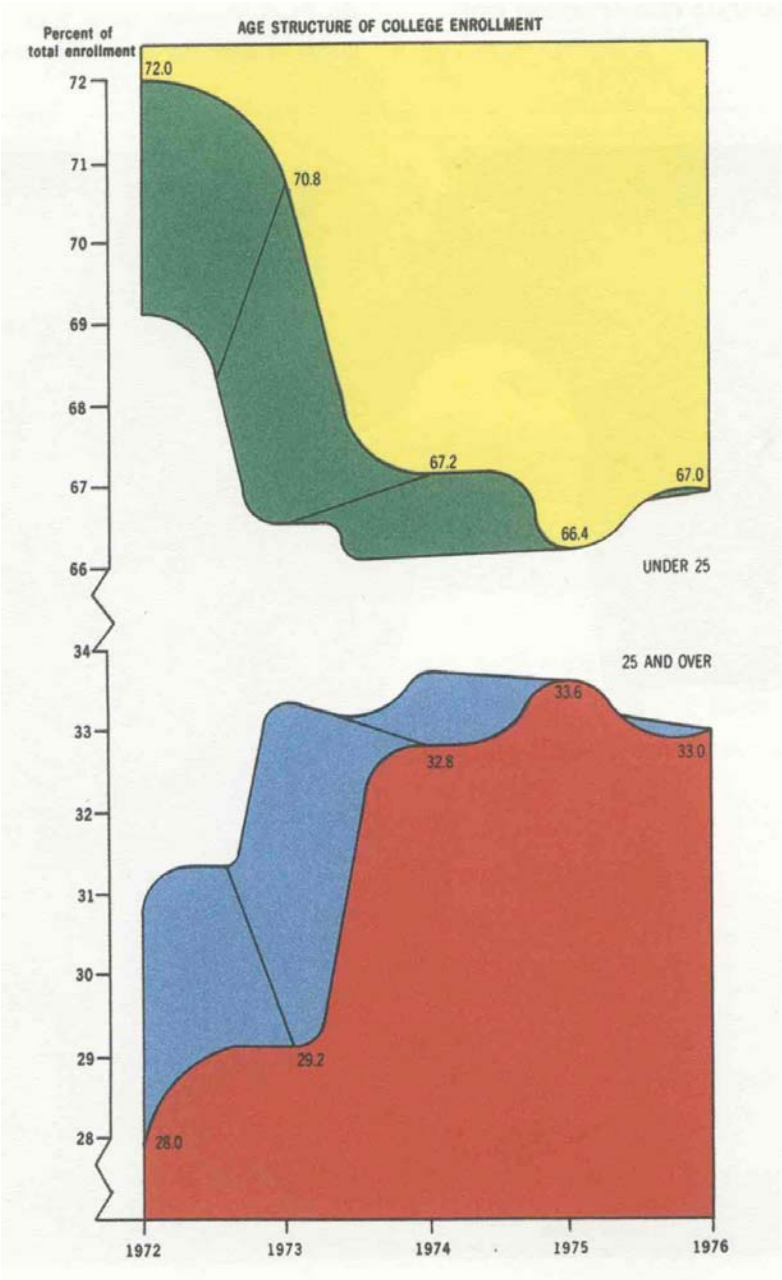

American Education (~1970)

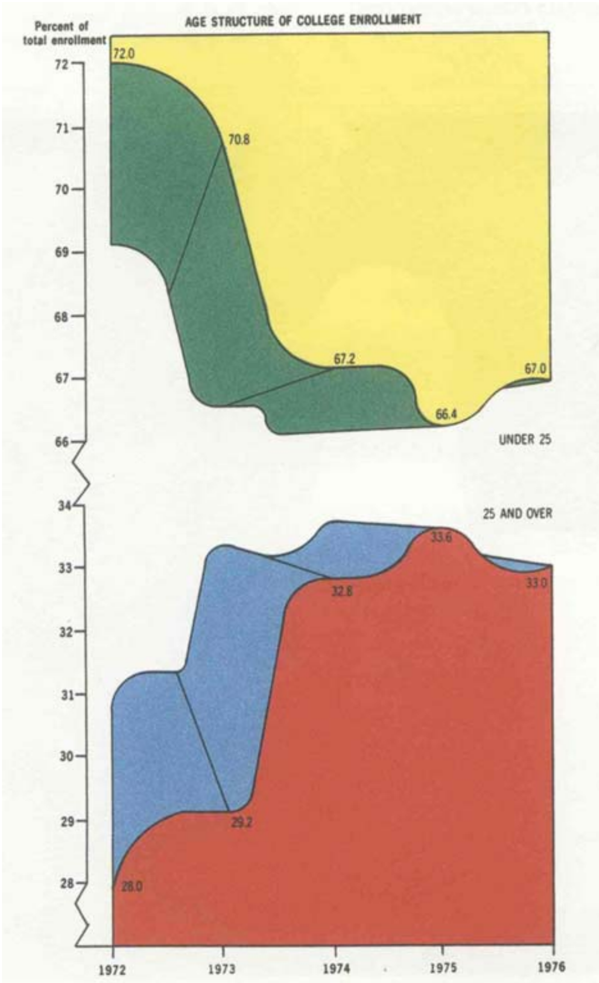

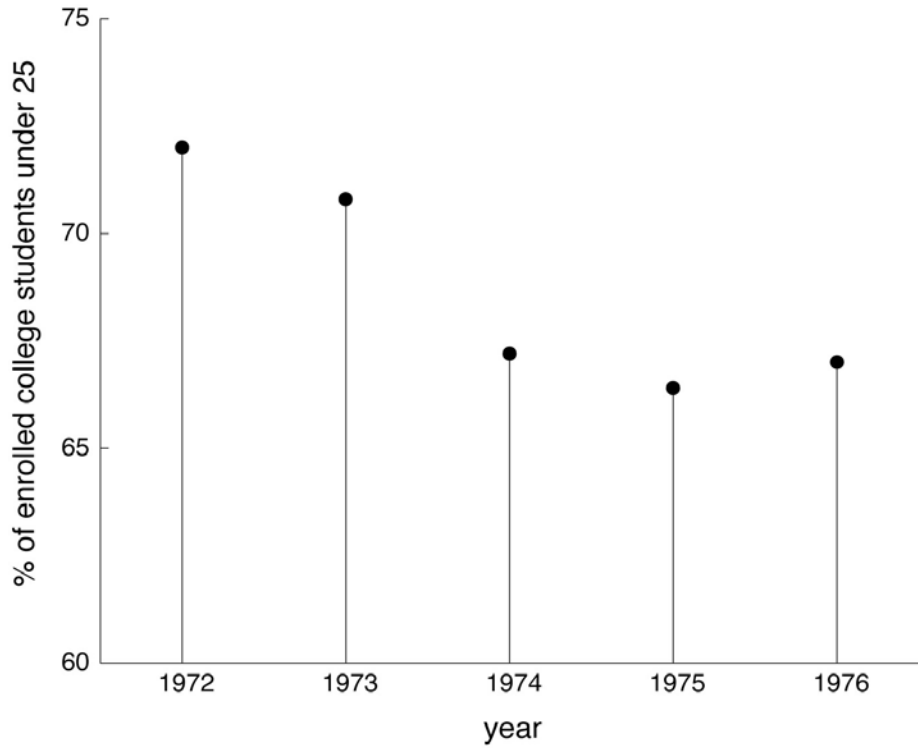

"This may well be the worst graphic ever to find its way into print."
- Edward Tufte

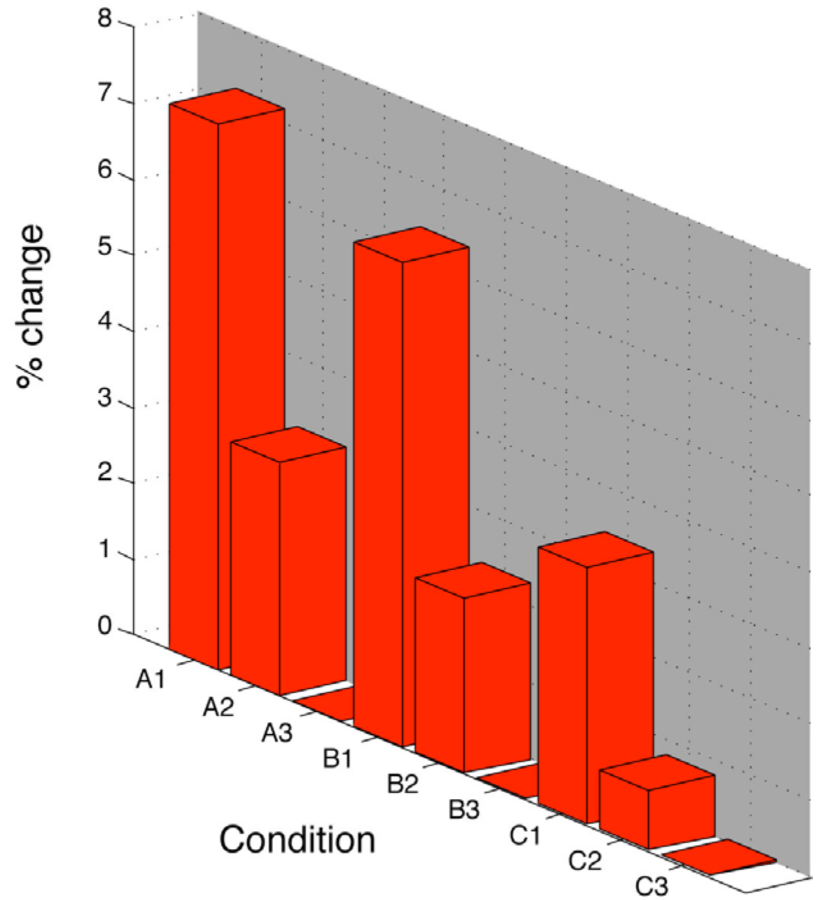

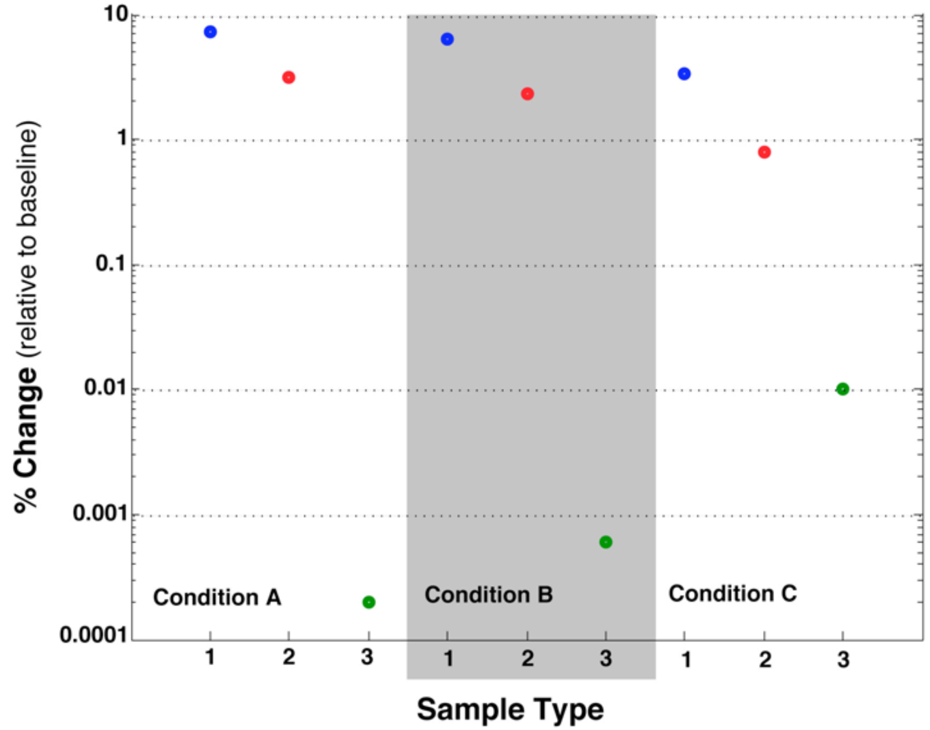

Further means to improve?

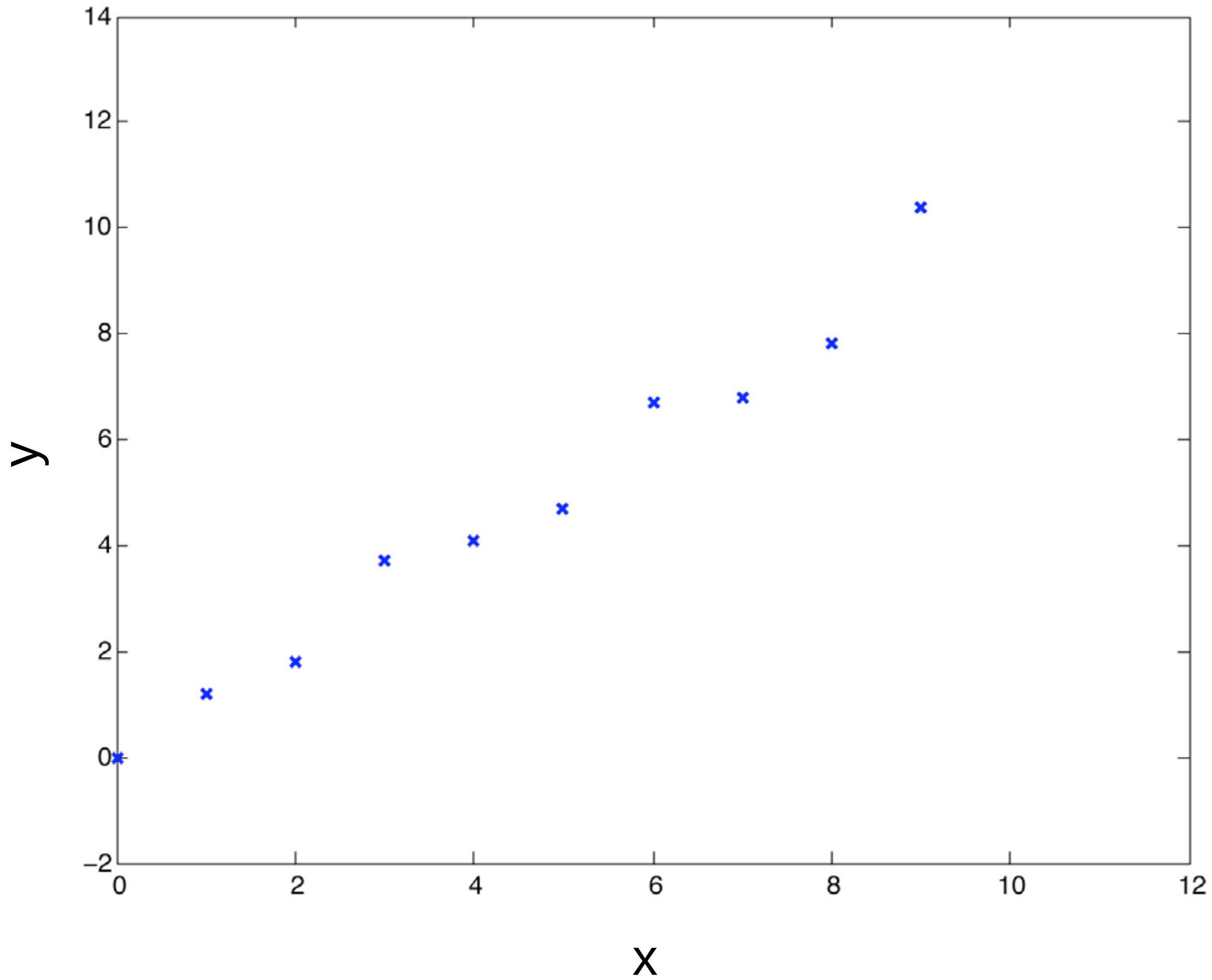

14
12
10
8
6
4
2
0
−2
0
2
4
6
8
10
12
y
x

Curve Fitting

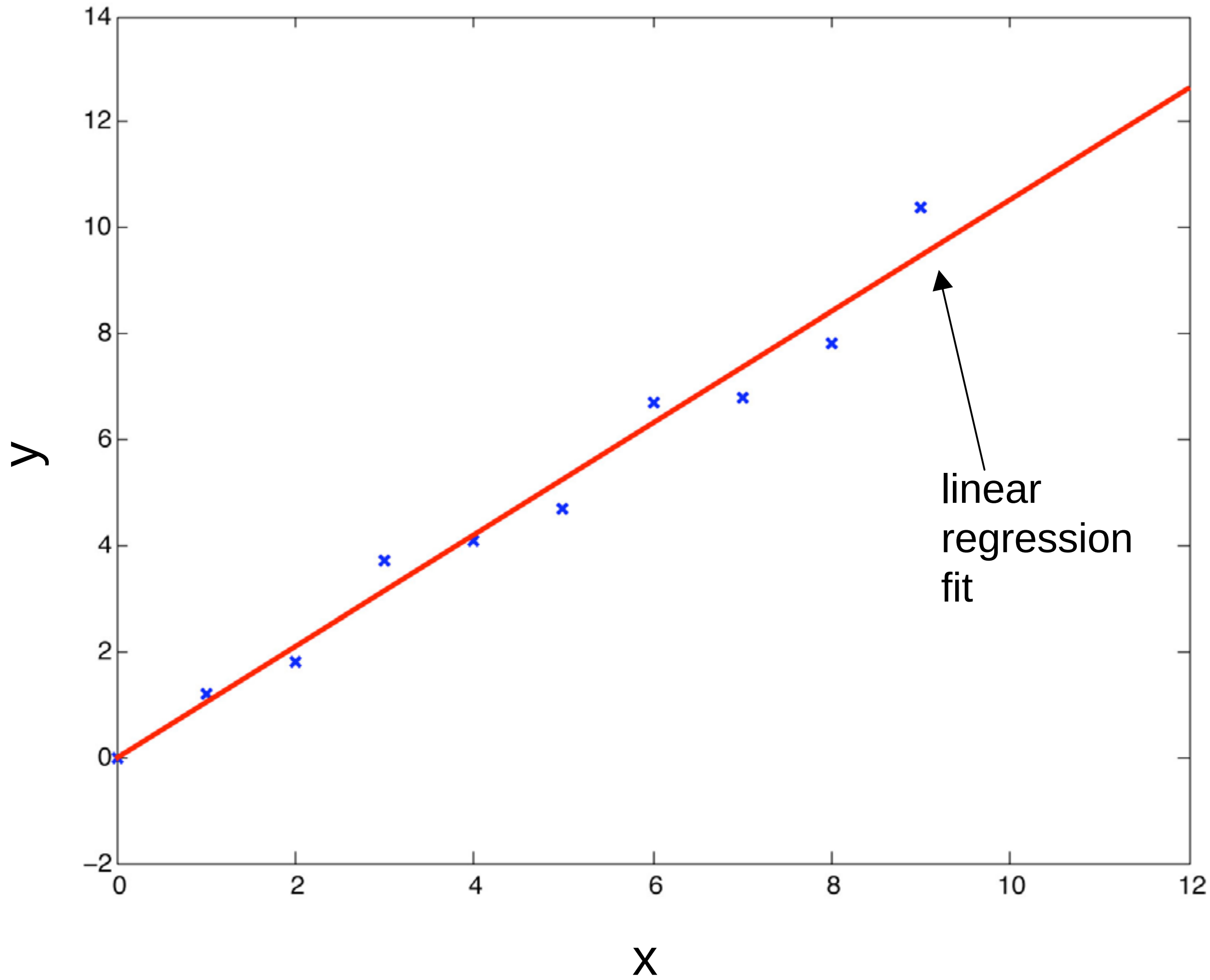

Curve Fitting ⇒ Use Statistics

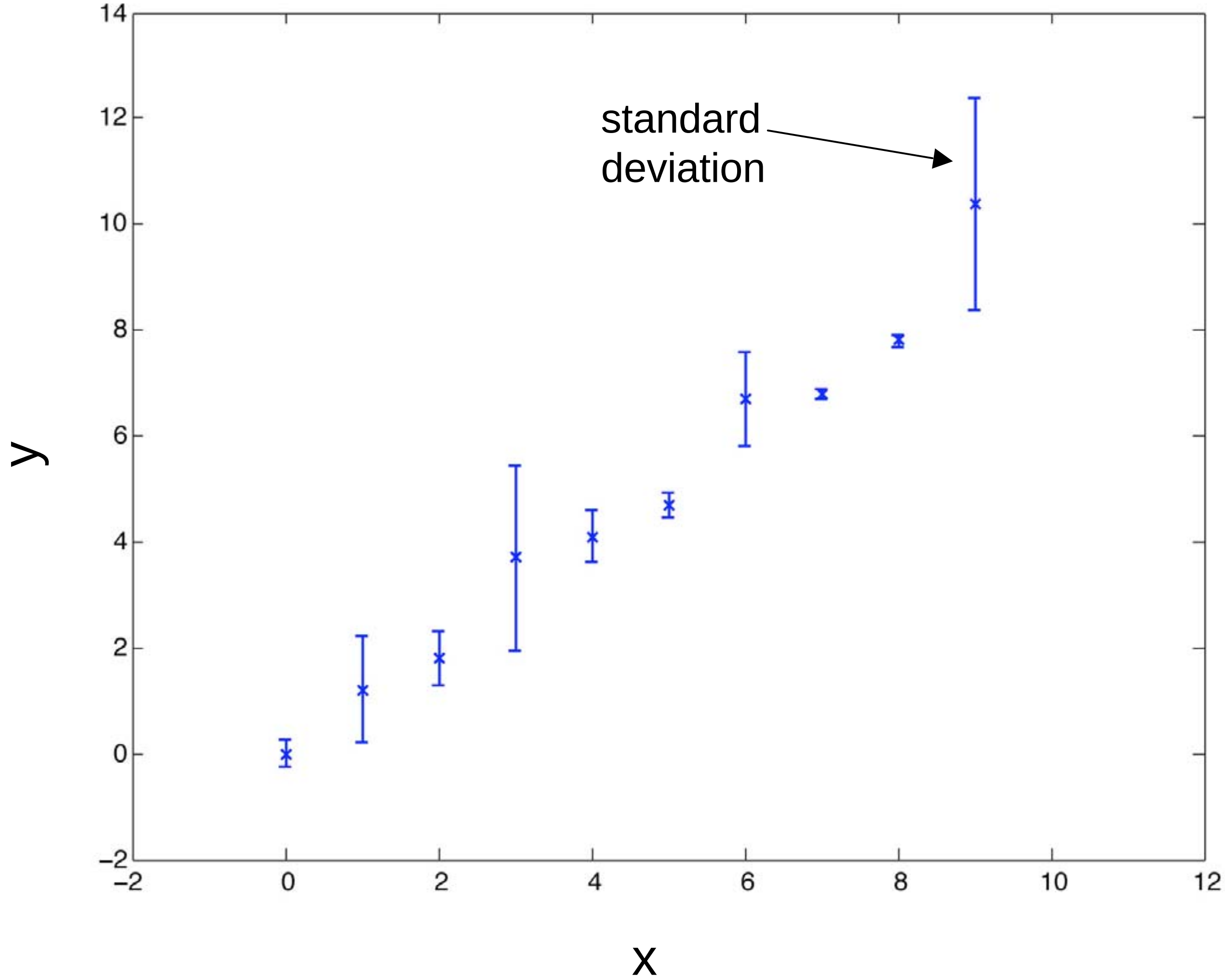

Curve Fitting ⇒ Use Statistics

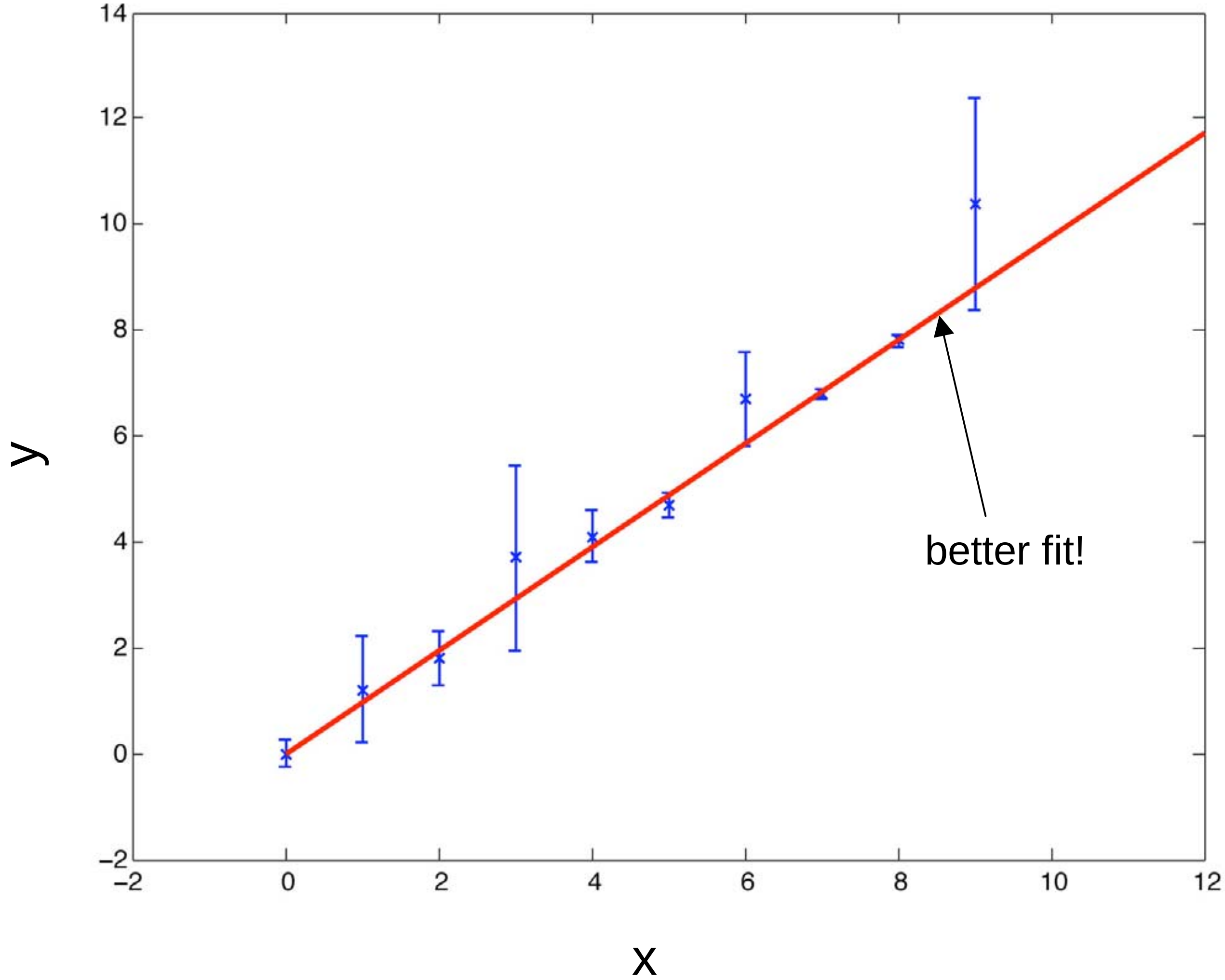

Curve Fitting ⇒ Use Statistics

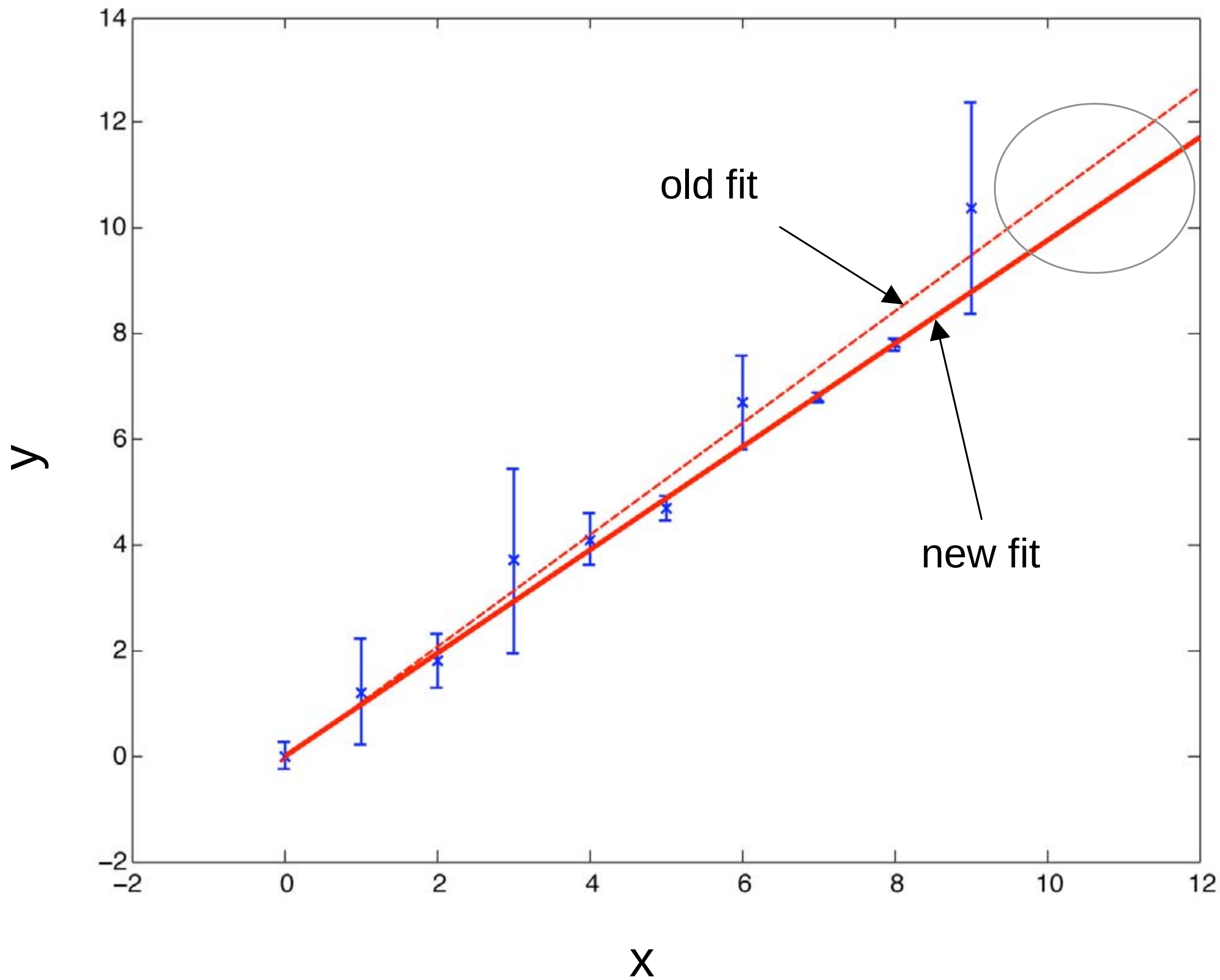

(Some) Common Pitfalls

Indefinite Antecedents

"Historically, it has been difficult to make direct physiological measurements at the level of the inner ear. This is because of the size, complex structure and sensitive nature of the cochlea (which for mammals is encased in the hardest bone in the body)."

(Some) Common Pitfalls

Indefinite Antecedents

?

"Historically, it has been difficult to make direct physiological measurements at the level of the inner ear. This is because of the size, complex structure and sensitive nature of the cochlea (which for mammals is encased in the hardest bone in the body)."

Jargon & Abbreviations

e.g. mRNA, mettaloenzymes, taxonomy, fitness, genetic *drift*, UBRP, et cetera

- Learn to use ⇔ But do not abuse!

- Think about possible etymological origins

Who is the author?

Did all these people really write this paper?

Vol 444 | 21/28 December 2006 | doi:10.1038/nature05390

nature

LETTERS

Observation of the radiative decay mode of the free neutron

Jeffrey S. Nico[1], Maynard S. Dewey[1], Thomas R. Gentile[1], H. Pieter Mumm[1], Alan K. Thompson[1], Brian M. Fisher[2], Isaac Kremsky[2], Fred E. Wietfeldt[2], Timothy E. Chupp[3], Robert L. Cooper[3], Elizabeth J. Beise[4], Kristin G. Kiriluk[4], James Byrne[5] & Kevin J. Coakley[6]

The theory of quantum electrodynamics (QED) predicts that beta decay of the neutron into a proton, electron and antineutrino should be accompanied by a continuous spectrum of soft photons. While this inner bremsstrahlung branch has been previously measured in nuclear beta and electron capture decay, it has never been observed in free neutron decay. Recently, the photon energy spectrum and branching ratio for neutron radiative decay have been calculated using two approaches: a standard QED framework[1–3] and heavy baryon chiral perturbation theory[4] (an effective theory of hadrons based on the symmetries of quantum chromodynamics). The QED calculation treats the nucleons as point-like, whereas the latter approach includes the effect of nucleon structure in a systematic way. Here we observe the radiative decay mode of free neutrons, measuring photons in coincidence with both the emitted electron and proton. We determined a branching ratio of $(3.13 \pm 0.34) \times 10^{-3}$ (68 per cent level of confidence) in the energy region between 15 and 340 keV, where the uncertainty is dominated by systematic effects. The value is consistent with the predictions of both theoretical approaches; the characteristic energy spectrum of the radiated photons, which differs from the uncorrelated background spectrum, is also consistent with the calculated spectrum. This result may provide opportunities for more detailed investigations of the weak interaction processes involved in neutron beta decay.

The neutron is composed of two down quarks and an up quark and is stable under the strong and electromagnetic interactions. The weak interaction, however, can convert a down quark into an up quark through the emission of a virtual *W* gauge boson that subsequently decays into an electron and an antineutrino. In QED, the decay is also accompanied by an inner-bremsstrahlung photon in the process:

$$n \rightarrow p + e^{-} + \bar{\nu}_e + \gamma.$$

QED takes into account the inner bremsstrahlung produced by the electron while the heavy baryon chiral perturbation theory approach includes the photon emission from the weak interaction vertex. Because direct emission from the weak vertex contributes less than 1% to the total intensity, both the photon energy spectrum and the polarization are dominated by the electron inner bremsstrahlung. The total intensity of inner bremsstrahlung diverges logarithmically as the photon energy E goes to zero because the spectrum displays the $1/E$ behaviour that is characteristic of all soft photon processes. However, it has long been established that this infrared divergence is cancelled in all orders of perturbation theory by higher-order virtual photon corrections to the radiationless mode[5–7].

The experimental challenge for the detection of radiative neutron decay is to distinguish the low rate of radiative decay events at observable energies from the intense photon background associated with a neutron beam. The estimated branching ratio above 15 keV is only about 3×10^{-3}, which, when coupled with the long neutron lifetime, makes the rate of detectable photons quite small. A previous experimental study of neutron radiative decay arrived at an upper limit of 6×10^{-3} at the 90% confidence level for the branching ratio for emission of photons with an energy between 35 and 100 keV (ref. 8). The report of a more recent experiment[9] was disputed[10] with compelling arguments. Our experiment was mounted at the NG-6 fundamental physics end-station at the Center for Neutron Research at the National Institute of Standards and Technology. It was designed to detect the coincidence of a photon and electron followed by a delayed proton, thereby reducing the probability of recording uncorrelated background events[11]. A strong magnetic field transported the electrons and protons away from the photon detector, which increased the solid angle for detection and minimized correlated backgrounds. The detection method used a solenoid design and proton detection scheme previously used to measure both the neutron lifetime[12,13] and the electron–antineutrino angular correlation coefficient[14]. An electrostatic mirror was used to vary the rate of detected electron–proton coincidences without changing the uncorrelated photon background rate, thus providing a signature for the detection of radiative decay and an important systematic check on possible backgrounds.

The NG-6 cold neutron beam entered beryllium-coated guides and collimation originally designed for use in a neutron time-reversal violation experiment[15] and adapted for this experiment by implementing slight changes in the beam optics. The collimation used a series of ^{6}LiF apertures backed with lead to define the beam, and the vacuum components were lined with ^{6}Li-glass to absorb scattered neutrons, thus significantly reducing background radiation. The beam entered parallel to the 4.6 T magnetic field produced by a superconducting solenoid. The detection scheme for the decay products is shown in Fig. 1. To satisfy the need for a large solid-angle photon detector that can operate in a strong magnetic field and at low temperatures, a system consisting of a scintillating crystal coupled to an avalanche photodiode was employed[16]. The photon was detected by a single bismuth germanate (BGO) crystal viewed by a silicon avalanche photodiode (APD). As the temperature decreases, the APD gain increases, its noise decreases[17], and the BGO light output increases[18]; these features allowed us to obtain a low-energy detection threshold of 15 keV. The BGO crystal was mounted in an aluminium

[1]Physics Laboratory, National Institute of Standards and Technology, Gaithersburg, Maryland 20899, USA. [2]Department of Physics, Tulane University, New Orleans, Louisiana 70118, USA. [3]FOCUS and Physics Department, University of Michigan, Ann Arbor, Michigan 48109, USA. [4]Department of Physics, University of Maryland, College Park, Maryland 20742, USA. [5]Department of Physics and Astronomy, University of Sussex, Brighton BN1 9QH, UK. [6]Information Technology Laboratory, National Institute of Standards and Technology, Boulder, Colorado 80305, USA.

N_2 and CO both occur in the same velocity component, that the velocity separation in O I and H_2 agree, and that the CO component is aligned in velocity with the higher-velocity O I component strongly supports our claim of the first detection of interstellar N_2. Our N_2 detection is further supported by the fact that the excitation temperatures of H_2 (1–0) and of N_2 agree for the longer-wavelength component. Although the N_2 b-value is not reliably determined, we use the S I b-value to improve our estimate and find $N(N_2) = (4.6 \pm 0.8) \times 10^{13}\,cm^{-2}$. We note that S I may be more extended than CO or N_2 in interstellar space. Because nitrogen has a lower cosmic abundance compared to either carbon or oxygen, we believe that $N(N_2)$ should not be larger than $N(CO)$ and should the true N_2 b-value be much smaller than that for S I (although this is unlikely), significant amounts of N_2 (that is, $N(N_2) > 10^{14}\,cm^{-2}$) could be present. Our firm lower limit to $N(N_2)$ is not sensitive to the b-value or the choice of stellar model used to represent the stellar continuum. Taken together, these data strongly indicate that N_2 has been detected for the first time in the interstellar medium and with a column density of $N(N_2) > 3.8 \times 10^{13}\,cm^{-2}$.

From our analysis of the O I line at 1,356 Å, we find $N(O\,I) = (6.77 \pm 0.50) \times 10^{17}\,cm^{-2}$ for the component near $3\,km\,s^{-1}$. Using the observed $N(O\,I)/N(H_{tot})$ ratio $(4.74 \pm 0.81) \times 10^{-4}$ (ref. 11), this component contains $N(H_{tot}) = 1.5 \times 10^{21}\,cm^{-2}$, where $N(H_{tot}) = N(H\,I) + 2N(H_2)$. The amount of interstellar reddening for this component can be determined from the dust-to-gas ratio[28], which yields $E(B-V) = 0.26\,mag^{-1}$. Assuming that the ratio of total to selective extinction is 3.1 (ref. 29), we find that the total visual extinction is 0.8 mag. When we compare our results to models of interstellar gas-phase chemistry[1], none of the standard cloud models explain our observations. The observed N_2 fractional abundance is more than two orders of magnitude too low for dense cloud models and approximately two orders of magnitude larger than expected from models of diffuse clouds. The fact that N I shows a deficiency in its relative abundance for lines of sight with $N(H_{tot}) > 10^{21}\,cm^{-2}$ would argue that dense cloud chemistry should be important for interstellar nitrogen. However, the measured N_2 abundance and upper limits for other sightlines[7] do not account for the observed variations. Additionally, we find that the fractional abundance of N_2 towards HD 124314 is $N_2/H_2 = 3.3 \times 10^{-7}$, similar to those estimated from N_2H^+ observations[4] of dark molecular clouds. Therefore, the far-ultraviolet lines of N_2 provide a unique probe of interstellar nitrogen chemistry in the transition region from diffuse to dense molecular gas. □

Received 16 February; accepted 30 April 2004; doi:10.1038/nature02614.

1. Viala, Y. P. Chemical equilibrium from diffuse to dense interstellar clouds. I Galactic molecular clouds. *Astron. Astrophys.* (Suppl.) **64,** 391–437 (1986).
2. Bergin, E. A., Langer, W. D. & Goldsmith, P. F. Gas-phase chemistry in dense interstellar clouds including grain surface molecular depletion and desorption. *Astrophys. J.* **441,** 222–243 (1995).
3. Womack, M., Ziruys, L. M. & Wyckoff, S. A survey of N_2H^+ in dense clouds: Implications for interstellar nitrogen and ion-molecule chemistry. *Astrophys. J.* **387,** 417–429 (1992).
4. Womack, M., Ziruys, L. M. & Wyckoff, S. Estimates of N_2 abundances in dense molecular clouds. *Astrophys. J.* **393,** 188–192 (1992).
5. Lutz, B. L., Owen, T. & Snow, T. P. Jr A search with *Copernicus* for interstellar N_2 in diffuse clouds. *Astrophys. J.* **227,** 159–162 (1979).
6. Sandford, S. A., Bernstein, M. P., Allamandola, L. J., Goorvitch, D. & Teixeira, T. C. V. S. The abundances of solid N_2 and gaseous CO_2 in interstellar dense molecular clouds. *Astrophys. J.* **548,** 836–851 (2001).
7. Knauth, D. C., Andersson, B.-G., McCandliss, S. R. & Moos, H. W. Potential variations in the interstellar N I abundance. *Astrophys. J.* **596,** L51–L54 (2003).
8. Le Petit, F., Roueff, E. & Herbst, E. H_3^+ and other species in the diffuse cloud towards ζ Persei: A new detailed model. *Astron. Astrophys.* **417,** 993–1002 (2004).
9. Walborn, N. R. The space distribution of the O stars in the solar neighborhood. *Astron. J.* **78,** 1067–1073 (1973).
10. Cruz-Gonzalez, C., Recillas-Cruz, E., Costero, R., Peimbert, M. & Torres-Peimbert, S. A catalogue of galactic O stars. The ionization of the low density interstellar medium by runaway stars. *Rev. Mex. Astron. Astrofis.* **1,** 211–259 (1974).
11. André, M. K. *et al.* Oxygen gas-phase abundance revisited. *Astrophys. J.* **591,** 1000–1012 (2003).
12. Perryman, M. A. C. *et al.* The *HIPPARCOS* catalogue. *Astron. Astrophys.* **323,** L49–L52 (1997).
13. Moos, H. W. *et al.* Overview of the *Far Ultraviolet Spectroscopic Explorer* mission. *Astrophys. J.* **538,** L1–L6 (2000).
14. Sahnow, D. J. *et al.* On-orbit performance of the *Far Ultraviolet Spectroscopic Explorer* satellite. *Astrophys. J.* **538,** L7–L11 (2000).
15. Dixon, W. V. & Sahnow, D. J. CalFUSE v2.2: An improved data calibration pipeline for the *Far Ultraviolet Spectroscopic Explorer (FUSE)* in astronomical data analysis software and systems XII. (Spec. Iss.; eds Payne, H.E., Jedrzejewski, R.I. & Hook, R. N.) *ASP Conf. Ser.* **295,** (2003) 241–244.
16. Knauth, D. C., Howk, J. C., Sembach, K. R., Lauroesch, J. T. & Meyer, D. M. On the origin of the high-ionization intermediate velocity gas toward HD 14434. *Astrophys. J.* **592,** 964–974 (2003).
17. Federman, S. R., Glassgold, A. E., Jenkins, E. B. & Shaya, E. J. The abundance of CO in diffuse interstellar clouds. An ultraviolet survey. *Astrophys. J.* **242,** 545–559 (1980).
18. Abgrall, H. & Roueff, E. Wavelengths, oscillator strengths and transition probabilities of the H_2 molecule for Lyman and Werner systems. *Astron. Astrophys.* (Suppl.) **79,** 313–328 (1989).
19. Abgrall, H., Roueff, E. & Viala, Y. Vibration-rotation transition probabilities for the ground electronic $X^1\Sigma^+$ state of HD. *Astron. Astrophys.* (Suppl.) **50,** 505–522 (1982).
20. Morton, D. C. Atomic data for resonance absorption lines. III. Wavelengths longward of the Lyman limit for the elements hydrogen to gallium. *Astrophys. J.* (Suppl.) **149,** 205–238 (2003).
21. Stark, G. *et al.* Line oscillator strength measurements in the 0–0 band of the $c_4'^1\Sigma_u^+ - X^1\Sigma_g^+$ transition of N_2. *Astrophys. J.* **531,** 321–328 (2000).
22. Conti, P. S. & Ebbets, D. Spectroscopic studies of O-type stars. VII. Rotational velocities *V sin i* and evidence for macroturbulent motions. *Astrophys. J.* **213,** 438–447 (1977).
23. Lanz, T. & Hubeny, T. A grid of non-LTE line-blanketed model atmospheres of O-type stars. *Astrophys. J.* (Suppl.) **146,** 417–441 (2003).
24. Sheffer, Y., Federman, S. R. & Andersson, B.-G. FUSE measurements of Rydberg bands of interstellar CO between 925 and 1150 Å. *Astrophys. J.* **597,** L29–L32 (2003).
25. Hedin, A. E. Extension of the MSIS thermospheric model into the middle and lower atmosphere. *J. Geophys. Res.* **96,** 1159–1172 (1991).
26. Clayton, R. N. Self shielding in the Solar Nebula. *Nature* **415,** 860–861 (2002).
27. Van Dishoeck, E. F. & Black, J. H. The photodissociation and chemistry of interstellar CO. *Astrophys. J.* **334,** 771–802 (1988).
28. Bohlin, R. C., Savage, B. D. & Drake, J. F. A survey of interstellar H I from L_α absorption measurements. II. *Astrophys. J.* **242,** 132–142 (1978).
29. Sneden, C., Gehrz, R. D., Hackwell, J. A., York, D. G. & Snow, T. P. Infrared colors and the diffuse interstellar bands. *Astrophys. J.* **223,** 168–179 (1978).

Supplementary Information accompanies the paper on **www.nature.com/nature**.

Acknowledgements We thank A. Fullerton, S. R. Federman, P. Feldman, E. B. Jenkins, P. Sonnentrucker and P. Wannier for discussions and G. Stark for sharing his unpublished N_2 f-values. This work is based on observations made with the NASA-CNES-CSA Far Ultraviolet Spectroscopic Explorer, which is operated for NASA by Johns Hopkins University.

Competing interests statement The authors declare that they have no competing financial interests.

Correspondence and requests for materials should be addressed to D.C.K. (dknauth@pha.jhu.edu).

A precision measurement of the mass of the top quark

DØ Collaboration*

*A list of authors and their affiliations appear at the end of the paper

The standard model of particle physics contains parameters—such as particle masses—whose origins are still unknown and which cannot be predicted, but whose values are constrained through their interactions. In particular, the masses of the top quark (M_t) and W boson (M_W)[1] constrain the mass of the long-hypothesized, but thus far not observed, Higgs boson. A precise measurement of M_t can therefore indicate where to look for the Higgs, and indeed whether the hypothesis of a standard model Higgs is consistent with experimental data. As top quarks are produced in pairs and decay in only about 10^{-24} s into various final states, reconstructing their masses from their decay products is very challenging. Here we report a technique that extracts more information from each top-quark event and yields a greatly improved precision (of $\pm 5.3\,GeV/c^2$) when compared to previous measurements[2]. When our new result is combined with our published measurement in a complementary decay mode[3] and with the only other measurements available[2], the new world average for M_t becomes[4] $178.0 \pm 4.3\,GeV/c^2$. As a

Energy-transfer pumping of semiconductor nanocrystals using an epitaxial quantum well

3 - Pitfalls

Use of Mathematical Equations

(don't be afraid!)

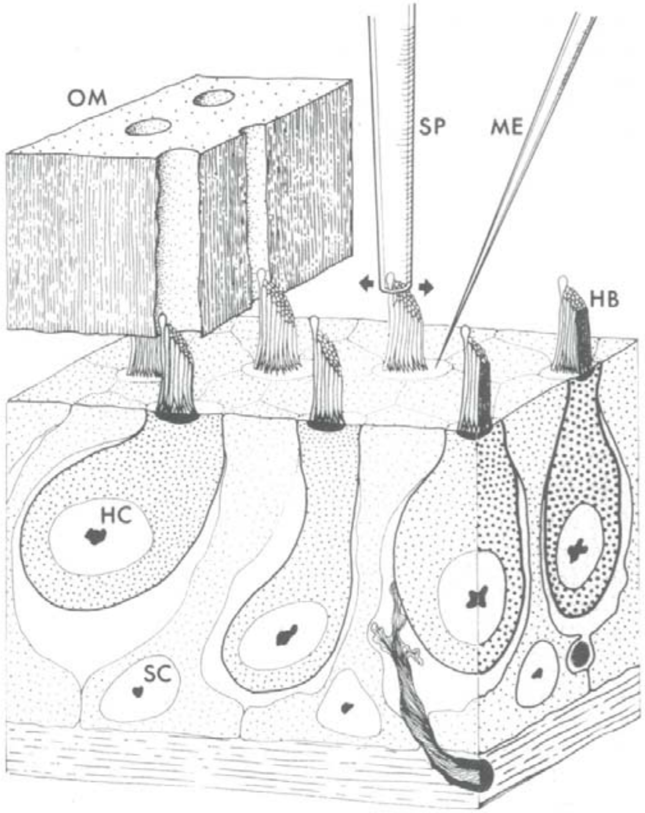

Corey and Hudspeth (1977)

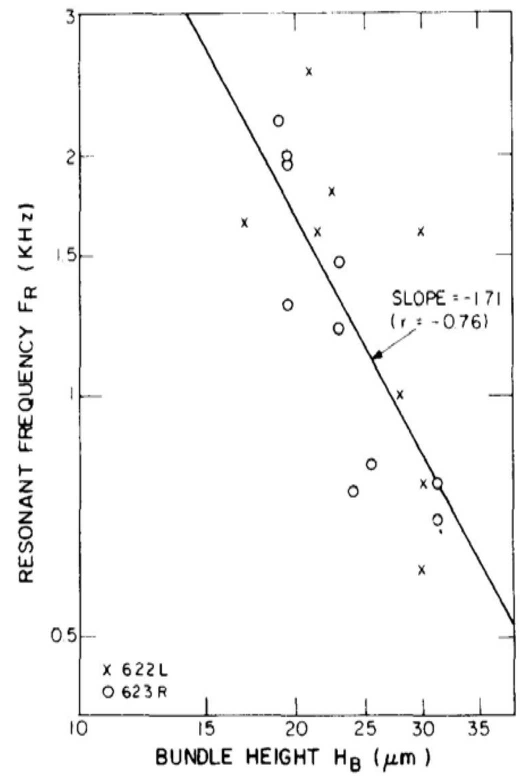

Frishkopf & DeRosier (1983)

$$m\ddot{x} + b\dot{x} + kx = A\sin\omega t$$

stiffness changes with bundle height

Summary

Style - find and develop your own

Graphics - use principles of *graphical excellence*

Pitfalls - learn to avoid common mistakes

References

Style:
- *Clear and Simple as the Truth* (Thomas and Turner)
- *The Craft of Research* (Booth, Colomb & Williams)

Graphics:
- *The Visual Display of Quantitative Information* (Edward R. Tufte)

Pitfalls:
- *The Art of Scientific Writing* (Ebel, Bliefert & Russey)

slides of this talk will be posted at www.math.arizona.edu/~cbergevin/

Fini